Atmos. Chem. Phys. Discuss., 12, 4031–4071, 2012
www.atmos-chem-phys-discuss.net/12/4031/2012/
doi:10.5194/acpd-12-4031-2012

Atmospheric Chemistry and Physics Discussions

Retrieval of aerosol optical depth over land based on a time series technique using MSG/SERIVI data

L. Mei[1,9], Y. Xue[1,2], G. de Leeuw[3,4,5], T. Holzer-Popp[6], J. Guang[1], Y. Li[1,9], L. Yang[7], H. Xu[1,9], X. Xu[8,9], C. Li[8,9], Y. Wang[1,9], C. Wu[1], T. Hou[8,9], X. He[1,9], J. Liu[1,9], J. Dong[1,9], and Z. Chen[8,9]

[1]State Key Laboratory of Remote Sensing Science, jointly sponsored by the Institute of Remote Sensing Applications of Chinese Academy of Sciences and Beijing Normal University, Institute of Remote Sensing Applications, Chinese Academy of Sciences, Beijing 100101, China
[2]Faculty of Computing, London Metropolitan University, 166-220 Holloway Road, London N7 8DB, UK
[3]Department of Physics, University of Helsinki, Helsinki, Finland
[4]Finnish Meteorological Institute, Climate Change Unit, Helsinki, Finland
[5]Netherlands Organisation for Applied Scientific Research TNO, Utrecht, The Netherlands
[6]German Remote Sensing Data Center, German Aerospace Center, Oberpfaffenhofen, 82234 Wessling, Germany
[7]School of Geography, Beijing Normal University, Beijing, China

[8] Center for Earth Observation and Digital Earth, Chinese Academy of Sciences, No. 9 Dengzhuang South Road, Haidian District, Beijing 100094, China
[9] Graduate University of the Chinese Academy of Sciences, Beijing 100049, China

Received: 20 September 2011 – Accepted: 24 January 2012 – Published: 3 February 2012

Correspondence to: L. Mei (meilinlu@163.com, yxue@irsa.ac.cn)

Published by Copernicus Publications on behalf of the European Geosciences Union.

Abstract

A novel approach for the joint retrieval of aerosol optical depth (AOD) and surface reflectance, using Meteosat Second Generation – Spinning Enhanced Visible and Infrared Imagers (MSG/SEVIRI) observations in two solar channels, is presented. The retrieval is based on a time series (TS) technique, which makes use of the two visible bands at 0.6 µm and 0.8 µm in three orderly scan times (15 min interval between two scans) to retrieve the AOD over land. Using the radiative transfer equation for plane-parallel atmospheres two coupled differential equations for the upward and downward fluxes are derived. The boundary conditions for the upward and downward fluxes at the top and at the bottom of the atmosphere are used in these equations to provide an analytic solution for the surface reflectance. To derive these fluxes, the aerosol single scattering albedo (SSA) and asymmetry factor are required to provide a solution. These are provided from a set of six pre-defined aerosol types with the SSA and asymmetry factor (g). We assume one aerosol type for a grid of $1^{\circ} \times 1^{\circ}$ and the surface reflectance changes little between two consequent scans. A k approximation was used in the inversion to find the best solution of atmospheric properties and surface reflectance. The algorithm makes use of numerical minimisation routines to obtain the optimal solution of atmospheric properties and surface reflectance by selection of the most suitable aerosol type from pre-defined sets. Also, it is assumed that the surface reflectance is little influenced by aerosol scattering at 1.6 µm and therefore the ratio of surface reflectances in the solar band for two consequent scans can be well-approximated by the ratio of the reflectances at 1.6 µm. A further assumption is that the surface reflectance varies only slightly over a period of 30 min.

A detailed analysis of the retrieval results show that it is suitable for AOD retrieval over land. Six Aerosol Robotic Network (AERONET) sites with different surface types were used for detailed analysis and 42 other AERONET sites were used for validation. From 445 collocations representing stable and homogeneous aerosol type, we found that >75 % of MSG-retrieved AOD values compared to AERONET observed values

ACPD

12, 4031–4071, 2012

with an error envelope of $\pm 0.05 \pm 0.15\tau$ and a high correlation ($R > 0.86$). The AOD datasets derived using the TS method with SEVIRI data was also compared with collocated AOD products derived from the NASA TERRA and AQUA MODIS data using the dark dense vegetation (DDV) method and the Deep Blue algorithms. Using the TS method, AOD could be retrieved for more pixels than with the NASA Deep Blue algorithm. The AOD values derived compare favourably.

1 Introduction

A crucial issue with using satellite images to retrieve aerosol properties is the difficulty of separating and explicitly describing contributions to the observed signal from reflections by the underlying surface and from back-scattering by semitransparent aerosol particles (Hsu et al., 2003; Martonchik, 2009; Govaerts et al., 2010). This problem is generally ill-posed or under-constrained. The problem is particularly challenging for satellite remote over land, especially over bright surfaces. In that case, the contribution of aerosols reflection to the signal observed by satellites is very small compared to the surface contribution, which introduces uncertainty into the process of aerosol properties retrieval.

Present-day approaches for satellite remote sensing of aerosol properties retrieval over land can be grouped into three main categories (Tang et al. 2005): (1) retrieval based on detection of aerosol over dark surfaces from single pass satellite images; (2) use contrast reduction (or the blurring effect) of images from satellite multi-passes and (3) polarization. The first approach has been widely applied to multi-spectral imagers such as the Moderate Resolution Imaging Spectroradiometer (MODIS) and the Sea-viewing Wide Field-of-view Sensor (SeaWiFS) and to multi-angle imagers such as the Along-Track Scanning Radiometer (ATSR) and the Multiangle Imaging Spectro-Radiometer (MISR). Among multi-spectral imagers, the Dark Dense Vegetation (DDV) method is the most popular algorithm. It relies primarily on the use of low reflectance pixels or dark targets with low reflectance (Kaufman, 1993; Kaufman et al., 1990;

ACPD
12, 4031–4071, 2012

Kaufman and Sendra, 1988) and requires prior knowledge of accurate ground surface reflectance (King et al., 1992). One major limitation of the MODIS DDV approach is that when the surface reflectance at 2.1 μm is above 0.15, no retrievals are performed and the assumption of transparency in this channel is not considered valid (Kaufman et al., 1997a; Hsu et al., 2004; Remer et al., 2005). The relationship of visible to 2.1 μm surface reflectance is improved as a function of geometry, surface type (Remer et al., 2001; Gatebe et al., 2001) and scattering angle (Levy et al., 2007b). For the retrieval over bright surfaces such as arid, semi-arid and urban areas, Hsu et al. (2004) developed the deep blue algorithm which uses the fact that in the blue spectral region the surface is much darker than at longer wavelengths. This approach has an estimated accuracy of 20–30 %.

In aerosol retrieval algorithms developed for multi-angular imagers it is often assumed that the wavelength dependence of the shape of the surface bidirectional reflectance distribution function is (BRDF) negligible in comparison with the wavelength dependence of the surface and atmospheric scattering properties (Flowerdew and Haigh, 1995). This assumption can be made because the scattering elements of the surface are much larger than the wavelengths used in the retrieval procedure, and therefore the angular variation of the surface reflectance is often dominated by wavelength-independent geometric effects (Grey et al., 2006). This approach is used in the dual view algorithm (Veefkind et al., 1999), and the Swansea algorithm (Grey et al., 2006), both using ATSR data and the MISR algorithm (Diner et al., 2005). North et al. (1999) developed this approach further by considering the variation of the diffuse fraction of light with the wavelength.

The second approach is quite popular for geostationary satellites. The main approach is to build a surface reflectance reference by selecting the second darkest image in a certain time period for each pixel to avoid the effect of shadow and then to perform aerosol retrieval over land based on Look-Up tables of Rayleigh corrected reflectances for various surface reflectances and aerosol models for a range of aerosol optical depths (AODs). Knapp et al. (2002, 2005) found that a 14-day period was a

ACPD
12, 4031–4071, 2012

good compromise for the length of the time series and the influence of changes in surface reflectance and aerosol loading. One limitation of this approach is that it does not work for pixels with mixture of different ground surface and retrieval values of AOD in some parts are negative. Mei et al. (2012) developed this approach based on the assumptions that top-of-atmosphere (TOA) reflectance increases with the aerosol load and that the surface reflectance over time changes very little over certain period of time. The contribution of the surface and an aerosol background were chosen based on Aerosol Robotic Network (AERONET) information, and both of them vary in a different way with time. The variation of surface reflection is somewhat predictable, based on solar angles and vegetation changes, but for aerosol it depend on the source regions and transport which are hard to predict.

The third approach is to use polarized observations. The key advantage of this approach is its ability to systematically correct for the ground contribution (Deuze et al., 1993, 2001; Herman et al., 1997). The main contribution of land surfaces to the TOA polarised portion of total reflected radiance at short wavelengths is generally smaller and less variable compared to that of the atmosphere and can be more easily modelled and removed in principle. However, this method is only suitable for large scattering (large aerosol loads), small aerosol particles (Deuze et al., 2001) or small phase angles (Rondeaux and Herman, 1991; Breon et al., 1995).

Although different approaches are initially designed for a certain sensor with different properties has become a trend. For example, a composite surface background map is suitable for geostationary satellites; the Deep Blue algorithm for MODIS observations is a similar approach "transplanted" from a composite method. Kim et al. (2008) developed an algorithm to retrieve aerosol optical depth (AOD) from a geostationary earth orbit (GEO) satellite using visible and mid-infrared (mid-IR) channels, although the primary approach may be similar to Low Earth Orbit (LEO) satellite. One advantage of different algorithms is that they can be used as a prior to improve retrieval accuracy. This is especially important for new sensors such as MSG/SEVIRI. Unlike traditional geostationary satellites, MSG/SEVIRI has three narrow spectral bands in

ACPD
12, 4031–4071, 2012

the solar spectrum (at 0.63, 0.81 and 1.64 µm), in addition to the wide HRV band. Previous researches have showed varieties of approaches for MSG/SEVIRI AOD retrieval. Some papers tried to retrieve AOD Thieuleux et al. (2005) and Bennouna et al. (2009) demonstrated a good AOD results compared with AERONET observation over ocean using MSG/SEVIRI. As to AOD retrieval over land surface, Popp (2007) used a "background method" which is not suitable for bright surface with absorbing aerosol to retrieve AOD from MSG/SEVIRI and Bernard et al. (2011) did an evaluation of this method, confirming that this method is suitable for most Europe area. Carrer et al. (2010) put forwarded daily estimates of aerosol optical thickness over land surface based on a directional and temporal analysis of MSG/SEVIRI visible observations. Govaerts et al. (2010) developed a joint retrieval method of surface reflectance and aerosol optical depth from MSG/SEVIRI observations with an optimal estimation approach. Meanwhile, Some mature retrieval algorithms were also "transplanted" for MSG/SEVIRI AOD retrieval, such as operational algorithm used to retrieve AOD over ocean for Advanced Very High Resolution Radiometer (AVHRR) (Brindley et al., 2005) and Oxford-RAL Aerosol and Cloud (ORAC) method (Claire et al., 2011).

In this paper, we present a novel method for AOD retrieval from MSG/SEVIRI data. The retrieval methodology is described in Sect. 2. The retrieval results are discussed in Sect. 4 following the introduction of data used for retrieval. Conclusions are presented Sect. 5.

2 Retrieval strategy

2.1 Retrieval method

The basic equation for the transfer of radiation in plane-parallel atmospheres can be written in the following form (Liou, 2002):

ACPD
12, 4031–4071, 2012

$$\mu\frac{dI(\tau,\Omega)}{d\tau} = I(\tau,\Omega) - \frac{\varpi}{4\pi}\int_{4\pi} I(\tau,\Omega')P(\Omega,\Omega')d\Omega' - \frac{\varpi}{4\pi}F_{\Theta}P(\Omega,-\Omega_0)\exp(-\frac{\tau}{\mu_0})$$
$$-(1-\varpi)B[T(\tau)] \quad (1)$$

A glossary of symbols used in this paper is given in the Appendix. Once the phase function has been expressed in terms of Legendre polynomials, Eq. (1) can be decomposed into two differential equations: one for the upward flux, and the other one for the downward flux. These equations are as follows:

$$\frac{dF^{\uparrow}(\tau)}{d\tau} = \gamma_1 F^{\uparrow}(\tau) - \gamma_2 F^{\downarrow}(\tau) - \gamma_3 \varpi F_{\Theta}\exp(-\frac{\tau}{\mu_0}) \quad (2)$$

$$\frac{dF^{\downarrow}(\tau)}{d\tau} = \gamma_1 F^{\uparrow}(\tau) - \gamma_1 F^{\downarrow}(\tau) - (1-\gamma_3)\varpi F_{\Theta}\exp(-\frac{\tau}{\mu_0}) \quad (3)$$

with the following boundary conditions for the upward and downward fluxes at the top and the bottom of the atmosphere,

$$\frac{F^{\uparrow}(\tau=0)}{F^{\downarrow}(\tau=0)} = A' \quad (4)$$

$$\frac{F^{\uparrow}(\tau=\tau_0)}{F^{\downarrow}(\tau=\tau_0)} = A \quad (5)$$

the following equation was derived:

$$A = \frac{[a+c(\Gamma-A')]e^{k\tau} + [b+c(A'\Gamma-1)]\Gamma e^{-k\tau} + (\Gamma^2-1)G^{+}e^{-\frac{\tau}{\mu_0}}}{[a+c(\Gamma-A')]\Gamma e^{k\tau} + [b+c(A'\Gamma-1)]e^{-k\tau} + (\Gamma^2-1)G^{-}e^{-\frac{\tau}{\mu_0}}} \quad (6)$$

where

$$a = G^{+} - G^{-}\Gamma \quad (7)$$

ACPD
12, 4031–4071, 2012

$$b = G^- - G^+\Gamma \tag{8}$$

$$c = F_\Theta \mu_0 \tag{9}$$

$$G^+ = \frac{\mu_0^2 \varpi F_\Theta}{(k\mu_0)^2 - 1}[(\gamma_1 - \frac{1}{\mu_0})\gamma_3 + \gamma_2\gamma_4] \tag{10}$$

$$G^- = \frac{\mu_0^2 \varpi F_\Theta}{(k\mu_0)^2 - 1}[(\gamma_1 + \frac{1}{\mu_0})\gamma_4 + \gamma_2\gamma_3] \tag{11}$$

$$k^2 = \gamma_1^2 - \gamma_2^2 \tag{12}$$

$$F_\Theta = S(\frac{r_0}{r})^2 \mu_0 \tag{13}$$

$$\Gamma = \frac{\gamma_1 - k}{\gamma_2} \tag{14}$$

$$\gamma_1 = \frac{1}{4}[7 - (4 + 3g)\varpi] \tag{15}$$

$$\gamma_2 = -\frac{1}{4}[1 - (4 - 3g)\varpi] \tag{16}$$

$$\gamma_3 = \frac{1}{4}(2 - 3g\mu_0) \tag{17}$$

$$\gamma_4 = 1 - \gamma_3 \tag{18}$$

For conservative scattering, $\omega = 1$. Simpler solutions can be derived with one of the eigenvalues. However, in the paper, we need two eigenvalues in order to get the relationship between reflectance and AOD. In practice, however, we may set $\omega = 0.999999$

ACPD
12, 4031–4071, 2012

in all equations above when there is non-absorbance and obtain the results for conservative scattering (Liou, 2002). For our model, we assume that the atmospheric optical depth consists of two parts: the molecular Rayleigh scattering ($\tau_{molecular}$), and the scattering of aerosol particles ($\tau_{aerosol}$). Therefore, the dimensionless quantity of the optical depth of the whole atmosphere is as follows:

$$\tau = \tau_{molecular} + \tau_{aerosol} \quad (19)$$

2.2 Aerosol model selection and update

The use of aerosol models results from the need to provide some prior information on the aerosol physical and chemical which determine their radiative properties (Govaerts et al., 2010). One absorption parameter (SSA) and one size parameter (g) are sufficient for representing the entire aerosol parameter space (Levy et al., 2007); Other parameters used are e.g. size information (such as mean radius) and optical properties (such as extinction/backscatter ration) (Omar et al., 2005), fine-mode fractions (FMF) (Kim et al., 2010). Govaerts et al. (2010) suggested six aerosol types (spherical non-absorbing, spherical moderately absorbing, spherical absorbing, non-spherical small, non-spherical medium and non-spherical large) that can be used in MSG/SEVIRI AOD retrieval. The aerosol models proposed by Govaerts et al. (2010) and the values of parameters describing each of them are presented in Table 1 and in Fig. 1.

2.3 Inverse problem

Modeling studies predict that, for certain pairs of wavelengths, the ratio of the bidirectional reflectance factor between wavelengths is approximately constant, irrespective of view direction (North et al., 1999). The angular variation of the surface reflectance is due to the macroscopic structure of the underlying surface (Flowerdew and Haigh, 1995), which is of a much larger scale than the wavelength of incident light (Curier et al., 2009). Therefore, the surface reflectance can be described by a part which describes the variation with wavelength and a part that describes the variations with geometry.

ACPD
12, 4031–4071, 2012

A geostationary satellite such as MSG revisits a certain location every 15 min and the geometry changes gradually throughout the day due to changes in solar radiations. In conditions of relatively stable aerosol loading, this property can be utilised to provide repeated views under different angles of illumination (Thomas et al., 2009). Under this assumption, the ratio of surface reflectance at two scan times can be written as follows:

$$k_\lambda = \frac{A_{1,\lambda}}{A_{2,\lambda}} \tag{20}$$

It shows that the grand mean absolute error with k-approximation is 3.8 % while Lambertian error is 14.5 % for predicted reflectance (Flowerdew and Haigh, 1995).

For most continental aerosol types, aerosol extinction decreases exponentially with wavelength; therefore, the AOD at 1.6 µm is usually small compared to the AOD in the visible spectrum (Curier et al., 2009). However, the SEVIRI 0.8 µm band includes a water vapour absorption band close to 0.83 µm. This may invalidate Eq. (19), so this band should be revised to remove the effect of water and other gases (http://modis.gsfc.nasa.gov/data/atbd/atmos_atbd.php).

$$A_\lambda^m = T_\lambda^{CO_2} T_\lambda^{O_3} T_\lambda^{H_2O} A'_\lambda \tag{21}$$

Because the SEVIRI scans the Earth disk every 15 min, the reflectance varies only slightly within the remaining solutions of the time-series (Knapp et al., 2005; Kim et al., 2008; Govaerts et al., 2010). The predefined aerosol type that fits the following equation is the true aerosol type.

$$\varepsilon = \min\{\sum_t \sum_{j=1}^{n} (A^k_{\lambda_{t,j}} - A^k_{\lambda_{t+1,j}})^2\} \tag{22}$$

In Eq. (22), t is different scan times, j is different solar bands and k is the number of predefined aerosol types.

Levy et al. (2007a) suggested that satellite images should map onto a $1^\circ \times 1^\circ$ grid while aerosol in one grid can be defined as one single type. We assumed that the

ACPD
12, 4031–4071, 2012

aerosol type in a restricted geographical area of 1° × 1° would be a single aerosol type. For each processed SEVIRI pixel, the solution was calculated independently for each predefined aerosol class. The details of all aerosol types in each pixel in an area of 1° × 1° were statistically analysed as following.

1. First, we assign one aerosol type from those six aerosol types for all pixels in the grid.

2. For each pixel in the grid, we calculate the surface reflectance using above method with three consequent scan SERIVI data. The Eq. (22) is used to calculate ε for the surface reflectance difference between two consequent scans. With our assumptions, the surface reflectance between two consequent scan times (15 min) should change little and ideally, ε should be zero.

3. We change the aerosol type and repeat (1) and (2) procedures. We can obtain six ε values for six aerosol types. We assume that the aerosol type with smallest ε value is the right aerosol type for the pixel in the grid and the aerosol type occurring most frequently was chosen as the most suitable aerosol type for the grid.

4. By repeating steps (1) to (3), we then obtained the aerosol type in the whole study area and reprocessed the AOD using the updated aerosol type.

3 Data

The MSG satellite can observe the Earth in 12 spectral channels with a resolution of 3 km at the sub-satellite point, providing image data which is critical for operational forecasting needs. A key feature of SEVIRI is its ability to continuously image the Earth every 15 min. Commonly, the reflectance $A(i)$ used in the retrieval algorithms, can be derived from the satellite-measured radiance assuming that the surface acts as

ACPD
12, 4031–4071, 2012

a Lambertian reflector and the atmosphere is horizontally uniform using the following equation:

$$A(i) = \frac{\pi \times L(i) \times d^2(t)}{I \times \cos(\theta(t,x))} \quad (23)$$

where $L(i)$ is the measured radiance in $\mathrm{mWm^{-2}\,sr^{-1}\,(cm^{-1})^{-1}}$, $d(t)$ is the Sun-Earth distance in astronomical units (AU) at time t, I is the band solar irradiance at 1 AU in $\mathrm{mWm^{-2}\,sr^{-1}\,(cm^{-1})^{-1}}$ (shown in Table 2), $\theta(t,x)$ is the solar zenith angle in radians at time t and location x and i is the channel number.

The AERONET sun photometer network has been developed to provide independent data for the validation of both airborne and space-borne aerosol observations (Holben et al., 1998). For the validation of the results from the TS altorithm, 42 sites were chosen for validation (Shown in Fig. 2). Table 3 shows information about the latitude, longitude, and elevation of the selected AERONET sites.

The middle wavelengths of MSG/SEVIRI visible bands are 0.6 and 0.8 µm, which are not available from the AERONET sun photometers. Therefore, the natural logarithm of AOD has been fitted as a quadratic polynomial of the natural logarithm of the wavelength (fitting error of about 0.01–0.02) (Eck et al., 1999) to provide the 0.6 and 0.8 µm AOD at the AERONET sites for validation of the MSG/SEVIRI AOD. Wavelengths of 0.44, 0.675 and 0.87 nm were selected for fitting:

$$\ln\tau_a(\lambda) = a_0 + a_1 ln\lambda + a_2(\ln\lambda)^2 \quad (24)$$

where $\tau_a(\lambda)$ is AOD at wavelength λ and a_0, a_1 and a_2 are polynomial coefficients.

4 Results and analysis

4.1 Time series of AOD

A spatial-temporary matching-up method (Choku et al., 2002; Remer et al., 2002, 2005; Chen et al., 2005) is used. We used the average value of a certain time (that is during

ACPD
12, 4031–4071, 2012

7.5 min before and 7.5 min after satellite overpass time) in different window size that is 1 × 1, 3 × 3 and 5 × 5, then we calculating the average and deviation value of different window size (1 × 1 need no calculation). If the average value of different not changes so much, we only use 1 × 1, otherwise, we choose the average value of certain window size with the smaller deviation. Forty-two AERONET sites were used for validation and a detailed analysis for the validation data was made to eliminate "outliers". Representative points were selected to provide arrange of surface types and aerosol models. As an example, shorter time-series (from 08:00 UTC to 18:00 UTC on 14 April 2010) of MSG/SEVIRI derived AOD at 0.8 µm and 0.6 µm and corresponding AERONET observations of AOD at six sites in Carpentras (5.058° E, 44.083° N), Hamburg (9.973° E, 53.568° N), Ispra (8.627° W, 45.803° N), Tamanrasset_INM (5.53° E, 22.79° N), Saada (8.156° W, 31.626° N) and IER_Cinzana (5.933867° E, 13.278433° N) are presented in Fig. 3. In general, there is good agreement at four sites between the MSG and AERONET estimated AOD for these two bands. For example, quite good agreement is found in Ispra during the whole day; 90 % of the values show differences smaller than 0.05. Note that the absolute error of typical AOD retrieval approaches is larger than 0.05 (Mishchenko et al., 2007). Occasionally, however, there are spikes in the MSG observations where AOD is overestimated or underestimated. For example, at 08:45 UTC, the MSG/SEVIRI AOD was greatly overestimated at Tamanrasset_INM; the MSG/SEVIRI AOD value was about twice the AERONET AOD value. This overestimation is most likely due to any residual cloud in a scene results in high AOD (de Leeuw et al., 2007). Additionally, the effect of residual gas absorption in the 0.8 µm band may also contribute to the high value. Most retrieval values were similar to AERONET values in Saada with the exception of two moments, 15:15 UTC and 17:00 UTC. The relative error at these two times was around 25 % compared with the AERONET results. The same situation was observed in Carpentras with several high retrieval AOD values, which were most likely due to incomplete cloud scressning.

A large error can be found in Hamburg in the morning and IER_Cinzana for the whole day. For Hamburg, a large error occurred at 09:00 UTC to 11:00 UTC (Fig. 3

ACPD
12, 4031–4071, 2012

– Hamburg). This large error may have been caused by a change in aerosol components, as described in Fig. 4. The fine mode fraction (FMF) at 0.5 µm fluctuated from 0.94 to 0.83 during the period from 09:00 UTC and 11:00 UTC, which implies that small particles are "inserted into" the atmosphere during this period. The change of aerosol components resulted in an incorrect choice of asymmetry factor and SSA (i.e. incorrect aerosol type). In addition, for IER_Cinzana, the MSG estimates of AOD were underestimated compared with the AERONET retrievals during the whole day. During this period, a large amount of vegetation burning was reported by MODIS Rapid Response System Global Fire Maps (http://rapidfire.sci.gsfc.nasa.gov/firemaps/). Consequently, smoke aerosol concentrations were high (typically with AOD greater than 1 at 0.6 µm) during this period and are clearly identified in both the MSG and AERONET retrievals. However, the MSG/SEVIRI AOD (around 0.8 at 0.6 µm) was lower than the AERONET AOD (around 1.2 at 0.6 µm); this result was primarily due to the incorrect aerosol type selection. Figure 4 demonstrates that the FMF in IER_Cinzana is small throughout the whole day and varies greatly from morning to afternoon. Because there are only six predefined aerosol types with fixed SSA and asymmetry factors, the six predefined SSA and asymmetry factors do not match well with the biomass burning aerosol type (mixture type). Levy et al. (2010) noted that some regions may be dominated by aerosol types that would not have been characterised by the clustering of available AERONET data. In short, the new model works well with a stable and homogenous aerosol type during retrieval time and the accuracy is higher with large particles such as dust (e.g. at the Tamanrasset_INM site).

The AOD retrieved by the TS method and the AOD at collocated AERONET sites are compared in Fig. 5. The linear regression yielded a gradient of 0.7682, an offset of 0.0546 with an R of 0.8604, and RMSE of 0.1917 at 0.8 µm and a gradient of 0.8386, an offset of 0.0481 with an R of 0.8756, and RMSE of 0.1826 at 0.6 µm. Most points are within the of 20 % error range (the blue dash line). For a higher AOD, approximately 60 % of points are within the 20 % error limit. Fig. 5 also shows that the TS algorithm works somewhat better at 0.6 µm than at 0.8 µm; this is especially

ACPD
12, 4031–4071, 2012

true at higher AOD because of the possible contamination by trace gas absorption at 0.8 µm and insufficient removal of this effect sign Eq. (22).The non-zero intercepts in the regressions result from an improper representation of surface reflectance in the MSG/SEVIRI retrieval procedure while the deviation of the slopes from unity indicates a systematic bias resulting primarily from an inappropriate choice of the aerosol model in the MSG/SEVIRI retrieval algorithm (Ichoku et al., 2002; Remer et al., 2004).

4.2 Satellite inter-comparisons

The different aerosol products vary as much as they do because so many assumptions are required at different stages of the processing schemes (Grey and North, 2009). One criterion for assessing a new algorithm is to compare the validation statistics of the new algorithm-derived results with the validation results of the other products (Melin et al., 2007), in particular the generally used MODIS aerosol products. Melin et al. (2007) and Mei et al. (2011) gave several rules for satellite inter-comparisons. Before doing comparison using scattering plot between MSG and MODIS, we firstly resized them into the same resolution that is 10 km × 10 km and then the nearest overpass time of MSG compared with TERRA/MODIS and AQUA/MODIS was chosen.As an example, Fig. 6 shows the comparisons by considering the satellite overpass time of study area of Terra and Aqua satellites between TS retrieval AOD and NASA aerosol products, including DDV and Deep Blue AOD products. It is noted that the MODIS and MSG/SEVIRI spectral ranges are slightly different. The effective wavelengths for the mid-visible bands are 0.55 and 0.6 µm for MODIS and SEVIRI, respectively. However, it is also useful to compare performances in this paper. Because there are no Deep Blue products of TERRA, we compare the DDV product of TERRA with MSG/SEVIRI at 11:00 UTC. We also compared DDV and Deep Blue products of AQUA and MSG/SEVIRI at 15:30 UTC. The caption of each figure gives the wavelength, resolution, time and algorithm information. It can be observed that the DDV method may fail to retrieve AOD in the study area because the reflectance is high, and some retrieval values may not reliable; the Deep Blue algorithm works much better

ACPD
12, 4031–4071, 2012

over bright surfaces. However, there are still many areas where the Deep Blue product does not provide and AOD value because some assumptions by DDV and Deep Blue algorithms did not apply in these areas. The TS method seems to work well over the whole area except in the presence of clouds. We also found that the AOD values in those study areas are always high (greater than 0.5 in many parts) because of the desert under-surface. The AOD distributions retrieved from MSG/SEVIRI and MODIS over the study area compare very well. However, in some areas, the TS method greatly underestimates the AOD; for example, in the southern part of Algeria, the AOD value retrieved by the TS method is low, which does not agree with the surrounding values. The primary reason for this underestimation may be an incorrect aerosol type selection because the aerosol here is a mixture of dust and biomass burning. In most areas, the trends of TS-derived AOD and the Deep Blue product fit well. The regression between AOD derived from the TS algorithm and the DDV product is shown in Fig. 7 while Fig. 8 displays the relationship between the TS method and the Deep Blue retrieved AODs. This result demonstrates that the TS method compares much better with the Deep Blue product than with that retrieved using the DDV method.

4.3 Aerosol type analysis

Without making assumptions about aerosol a priori it is not possible to infer aerosol optical properties from current satellite retrievals (Bulgin et al., 2011). Six aerosol type was predefined by single scattering albedo and asymmetry factor, they are Spherical Non Absorbing, Spherical Moderately Absorbing, Spherical Absorbing, Non Spherical Small, Non Spherical Medium and Non Spherical Large. Then retrieval cost function showed as Eq. (22) was used with prior knowledge of aerosol spatial distribution and surface temporary variation to accurately classify aerosol and get the best aerosol type during retrieval. Figure 9 demonstrated the aerosol type distribution over Africa area on 14 October 2010. Two dominant aerosol types were found over this region, which are Spherical Absorbing and Non Spherical Large, different ration of these two types corresponded to dust aerosol type and biomass burning aerosol type. Upper-Left of

ACPD
12, 4031–4071, 2012

all sub-maps in Fig. 9 showed that these two aerosol types are consistently collocated along the African coast. More evidence is needed to suggest that dust and biomass burning aerosol are directly mixed (Bulgin et al., 2011). We can also find that the absorption character (Spherical Absorbing with $\omega = 0.862$) is more obvious in the morning while the scattering character (Non Spherical Large with $\omega = 0.965$) is dominant in the late afternoon. Meanwhile, the distinguish of aerosol type is much more obvious in the morning and in the afternoon, for instant, in the morning, Spherical Absorbing aerosol type purely appeared in the north part while the Non Spherical Large aerosol type was purely in the south part, however, in the middle day, more aerosol type such as Spherical Moderately Absorbing and Non Spherical Small were mixed, because the longer path through the atmosphere in the morning and afternoon enhance the contribution the signal reflected by aerosols (Wagner et al., 2010), stronger effect aerosol type is strong enough to cover other aerosol effect.

5 Conclusions

A novel method has been proposed to simultaneously retrieve aerosol load and surface reflectance using SEVIRI observations. Six aerosol types were predefined, including both spherical and non-spherical types, and the absorption was included in these aerosol types. We confined our consideration to one approximate method, which reduced the problem to solving a set of differential equations in the application to shortwave radiation transfer. After approximating the exact integrodifferential equation of radioactive transfer equations for radiative equation by common differential equations for the upward and incident radiation fluxes, a relationship between the ground surface reflectance and apparent reflectance was proposed.

The algorithm has been proven to be capable of separating the aerosol contribution from the surface contribution in the overall TOA observed signal. The example results demonstrate that the TS algorithm shows good agreement with ground-based measurements of AOD as well as with current operational satellite aerosol products. The generic nature of the algorithm makes it suitable for a wide range of instruments.

ACPD
12, 4031–4071, 2012

However, the plane parallel radiative transfer used in the model restricts the solar zenith angle range from 0 to 80. The predefined aerosol types in this paper should be improved in the future to cover a variety of atmospheric events such as biomass burning. Although this preliminary validation is encouraging, the difference in wavelengths and the time differences of various collection methods make comparisons difficult, and further validation is needed. The paper pays more attention to the AOD retrieval and analysis, and the detailed analysis of reflectance will be given in the next paper.

Appendix A

List of symbols

I	Intensity of the radiation
Ω	Direction (zenith angle, azimuth angle)
τ	Aerosol optical depth
τ_0	Total atmosphere aerosol optical depth
ϖ	Single scattering albedo
F_Θ	Solar flux density at the top of the atmosphere when the instantaneous distance between the earth and sun is r
r	Earth-sun distance
P	Phase function
B	Planck function
T	Absolute temperature
$F^\uparrow$	Total upward flux densities
$F^\downarrow$	Total downward flux densities
A	Earth's surface reflectance
A'	Earth's system reflectance (apparent reflectance observed from space)

ACPD
12, 4031–4071, 2012

g	Asymmetry factor
α	Wavelength exponent in angstrom's turbidity formula
β	Angstrom's turbidity coefficient
ε	Backscattering coefficient
θ	Solar zenith angle
λ	Wavelength
$\tau_{\text{molecular}}$	Rayleigh optical depth
T_λ	Transmissivity at λ

Acknowledgements. This work was supported in part by the Ministry of Science and Technology (MOST) of China under Grant Nos. 2010CB950802 and 2010CB950803, and by the State Key Laboratory of Remote Sensing Science Innovation Program. L. L. Mei would like to thank the Director Prize under Grant No. Y1S02400CX from the Institute of Remote Sensing Applications of Chinese Academy of Sciences. The contribution of Gerrit de Leeuw was in part supported by the ESA-ESRIN project STSE-ALANIS Atmosphere Land Interaction Study, Theme 3 Aerosols. The authors would like to thank Yves M. Govaerts from EUMETSAT for his help with aerosol type selection. MSG data were available through EUMETSAT, and MODIS data were available through NASA MODIS LAADS. Many thanks are due to the principal investigators of the AERONET sites used in this paper for maintaining their sites and making their data publicly available, and to the AERONET coordination team for organizing and maintaining excellent and essential support for satellite retrieval development and validation.

References

Bernard, E., Moulin, C., Ramon, D., Jolivet, D., Riedi, J., and Nicolas, J.-M.: Description and validation of an AOT product over land at the 0.6 µm channel of the SEVIRI sensor onboard MSG, Atmos. Meas. Tech., 4, 2543–2565, doi:10.5194/amt-4-2543-2011, 2011.

Bennouna, Y. S., de Leeuw, G., Piazzola, J., and Kusmierczyk-Michulec, J.: Aerosol remote sensing over the ocean using MSG-SEVIRI visible images, J. Geophys. Res., 114, D23203, doi:10.1029/2008JD011615, 2009.

ACPD
12, 4031–4071, 2012

Breon, F. M., Tanre, D., Leconte, P. and Herman, M.: Polarized Reflectance of Bare Soils and Vegetation Measurements and Models, IEEE T. Geosci. Remote, 33, 487–499, 1995.
Brindley, H. E. and Ignatov, A.: Retrieval of mineral aerosol optical depth and size information from eteosat Second Generation SEVIRI solar reflectance bands, Remote Sens. Environ., 102, 344–363, 2006.
Bulgin, C. E., Palmer, P. I., Merchant, C. J., Siddans, R., Gonzi, S., Poulsen, C. A., Thomas, G. E., Sayer, A. M., Carboni, E., Grainger, R. G., Highwood, E. J., and Ryder, C. L.: Quantifying the response of the ORAC aerosol optical depth retrieval for MSG SEVIRI to aerosol model assumptions, J. Geophys. Res., 116, D05208, doi:10.1029/2010JD014483, 2011.
Chen, B. and Yang, Y.: MODIS aerosol optical thickness validation around Taiwan Strait and adjacent region, ACTA Oceanologica Sinica, 27, 170–176, 2005.
Carrer, D., Roujean, J. L., Hautecoeur, O., and Elias, T.: Daily estimates of aerosol optical thickness over land surface based on a directional and temporal analysis of SEVIRI MSG visible observations, J. Geophys. Res., 115, D10208, doi:10.1029/2009JD012272, 2010.
Curier, L., de Leeuw, G., Kolmonen, P., Sundstrom, A.-M., Sogacheva, L., and Bennouna, Y.: Aerosol retrieval over land using the (A)ATSR dual-view algorithm, in: Satellite Aerosol Remote Sensing over Land, edited by: Kokhanovsky, A. A. and de Leeuw, G., Chichester, UK: Praxis Publishing, 135–160, 2009.
de Leeuw, G., Schoemaker, R., Curier, L., Bennouna, Y., Timmermans, R., Schaap, M., Builtjes, P., and Koelemeijer, R.: AATSR derived aerosol properties over land. In Proceedings of ENVISAT Symposium 2007 held at Montreux, Switzerland, 23–27 April 2007 (ESA SP-636, July 2007), 2007.
Deuze, J. L., Breon, F. M., Roujean, J. L., Deschamps, P. Y., Devaux, C., Herman, M., and Podaire, A.: Analysis of POLDER Airborne Instrument Observations over Land Surfaces, Remote Sens. Environ., 45, 137–154, 1993.
Deuze, J. L., Breon, F. M., Devaux, C., Goloub, P., Herman, M., Lafrance, B., Maignan, F., Marchand, A., Nadal, F., Perry, G., and Tanre, D.: Remote sensing of aerosol over land surfaces from POLDER-ADEOS-1 polarized measurements, J. Geophys. Res., 106, 4913–4956, 2001.
Diner, D. J., Martonchik, J., Kahn, R. A., Pinty, B., Gobron, N., Nelson, D. L., and Holben, B. N.: Using angular and spectral shape similarity constraints to improve MISR aerosol and surface retrievals over land, Remote Sens. Environ., 94, 155–171, 2005.
Eck, T. F., Holben, B. N., and Reid, J. S.: Wavelength dependence of the optical depth of

ACPD
12, 4031–4071, 2012

biomass burning, urban, and desert dust aerosol, J. Geophys. Res., 104, 31333–31349, 1999.
Flowerdew, R. J. and Haigh, J. D.: An approximation to improve accuracy in the derivation of surface reflectances from multi-look satellite radiometers, Geophys. Res. Lett., 22, 1693–1696, 1995.
Gatebe, C. K., King, M. D., Tsay, S. C., Ji, Q., Thomas, A. G., and Li, J. Y.: Sensitivity of off-nadir zenith angles to correlation between visible and near-infrared reflectance for use in remote sensing of aerosol over land, IEEE T. Geosci. Remote, 39, 805–819, 2001.
Grey, W. M. F., North, P. R. J., Los, S. O., and Mitchell, R. M.: Aerosol optical depth and land surface reflectance multi-angle AATSR measurements: global validation and inter-sensor comparisons, IEEE T. Geosci. Remote, 44, 2184–2197, 2006.
Gery, W. M. F. and North, P. R. J.: Aerosol optical depth from dual-view (A)ATSR satellite observations, in: Satellite Aerosol Remote Sensing over Land, edited by: Kokhanovsky, A. A. and de Leeuw, G., Chichester, UK: Praxis Publishing, 161–192, 2009.
Govaerts, Y. M., Wagner, S., Lattanzio, A., and Watts, P.: Joint retrieval of surface reflectance and aerosol optical depth from MSG/SEVIRI observations with an optimal estimation approach: 1. Theory, J. Geophys. Res., 115, D02203, doi:10.1029/2009JD011779, 2010.
Hall, D. K., Riggs, G. A., and Salomonson, V. V.: Development of methods for mapping global snow cover using Moderate Resolution Imaging Spectroradiometer data, Remote Sens. Environ., 54, 127–140, 1995.
Herman, M., Deuze, J. L., Devaux, C., Goloub, P., Breon, F. M., and Tanre, D.: Remote Sensing of Aerosol over Land Surfaces Including Polarization Measurements and Application to POLDER Measurements, J. Geophys. Res., 102, 17039–17049, 1997.
Holben, B. N., Eck, T. F., Slutsker, I., Tanré, D., Buis, J. P., Setzer, A., Vermote, E., Reagan, J. A., Kaufman, Y. J., Nakajima, T., Lavenu, F., Jankowiak, I., and Smirnov, A.: AERONET – A federated instrument network and data archive for aerosol characterization, Remote Sens. Environ., 66, 1–16, 1998.
Hsu, N. C., Tsay, S. C., King, M. D., and Herman, J. R.: Aerosol Properties over Bright Reflecting Source Regions, IEEE T. Geosci. Remote, 42, 557–569, 2004.
Ichoku, C., Chu, D. A., Mattoo, S., Kaufman, Y. J., Remer, L. A., Tanre, D., Slutsker, I., and Holben, B. N.: A spatio-temporal approach for global validation and analysis of MODIS aerosol products, Geophys. Res. Lett., 29, 1616, doi:10.1029/2001GL013206, 2002.
Kaufman, Y. J.: Measurements of the aerosol optical thickness and the path radiance - Im-

ACPD
12, 4031–4071, 2012

plications on aerosol remote sensing and atmospheric corrections, J. Geophys. Res., 98, 2677–2692, 1993.
Kaufman, Y. J. and Sendra, C.: Algorithm for atmospheric corrections, Int. J. Remote Sens., 9, 1357–1381, 1988.
Kaufman, Y. J., Fraser, R. S., and Ferrare, R. A.: Satellite measurements of large-scale air pollution: Method, J. Geophys. Res., 95, 9895–9909, 1990.
Kaufman, Y. J., Tanre, D., Remer, L. A., Vermote, E. F., Chu, A., and Holben, B. N.: Operational remote sensing of tropospheric aerosol over land from EOS moderate resolution imaging spectroradiometer, J. Geophys. Res., 102, 17051–17067, doi:10.1029/96JD03988, 1997.
Kim, J., Yoon, J. M., Ahn, M. H., Sohn, B. J., and Lim, H. S.: Retrieving aerosol optical depth using visible and mid-IR channels from geostationary satellite MTSAT-1R, Int. J. Remote Sens., 29, 6181–6192, 2008.
Kim, J., Lee, J., Song, C. H., Kim, S., Chun, Y., Sohn, B., and Holben, B. N.: Characteristics of aerosol types from AERONET sunphotometer measurements, Atmos. Environ., 44, 3110–3117, 2010.
King, M. D., Kaufman, Y. J., Menzel, P., and Tanre, D.: Remote sensing of cloud, aerosol and water vapor properties from the Moderate Resolution Imaging Spectrometer (MODIS), IEEE T. Geosci. Remote, 30, 1–27, 1992.
Knapp, K. R. and Vonder Haar, T. H.: Aerosol optical depth retrieval from GOES-8: Uncertainty study and retrieval validation over South America, J. Geophys. Res.-Atmos., 107,4055, doi:10.1029/2001JD000505, 2002.
Knapp, K. P., Frouin, R., Kondragunta, S., and Prados, A.: Toward aerosol optical depth retrieval over land from GOES visible radiances: determining surface reflectance, Int. J. Remote Sens., 26, 4097–4116, 2005.
Levy, R. C., Remer, L. A., and Dubovik, O.: Global aerosol optical properties and application to Moderate Resolution Imaging Spectroradiometer aerosol retrieval over land, J. Geophys. Res., 112, D13210, doi:10.1029/2006JD007815, 2007a.
Levy, R. C., Remer, L., Mattoo, S., Vermote, E. F., and Kaufman, Y. J.: Second-generation algorithm for retrieving aerosol properties over land from MODIS spectral reflectance, J. Geophys. Res., 112, D13211, doi:10.1029/2006JD007811, 2007b.
Levy, R. C., Remer, L. A., Kleidman, R. G., Mattoo, S., Ichoku, C., Kahn, R., and Eck, T. F.: Global evaluation of the Collection 5 MODIS dark-target aerosol products over land, Atmos. Chem. Phys., 10, 10399–10420, doi:10.5194/acp-10-10399-2010, 2010.

ACPD
12, 4031–4071, 2012

Liou, K. N.: An Introduction to Atmospheric Radiation Second Edition, New York: Academic Press, 2002.
Martonchik, J. V., Kahn, R. A., and Diner, D. J.: Retrieval of aerosol properties over land using MISR observations, in: Satellite Aerosol Remote Sensing over Land, edited by: Kokhanovsky, A. A. and de Leeuw, G., Chichester, UK: Praxis Publishing, 267–268, 2009.
Mei, L. L., Xue, Y., Wang, Y., Hou, T. T., Guang, J., Li, Y. J., Xu, H., Wu, C. L., He, X. W., Dong, J., and Chen, Z. Q.: Prior information supported aerosol optical depth retrieval using FY2D data, in: Proceedings of IEEE/IGARSS to be held at Vancouver, Canada, 24–29 July, 2011.
Mei, L. L., Xue, Y., Xu, H., Guang, J., Li, Y. J., Wang, Y., Ai, J. W., Qi, Y., and He, X. W.: Validation and analysis of optical thickness retrieval over land, Int. J. Remote Sens., 33,781–803, 2012.
Melin, F., Zibordi, G., and Djavidnia, S.: Development and validation of a technique for merging satellite derived aerosol optical depth from SeaViFS and MODIS, Remote Sens. Environ., 108, 436–450, 2007.
Mishchenko, M. I., Geogdzhayev, I. V., Rossow, W. B., Cairns, B., Carlson, B. E., Lacis, A. A., Liu, L., and Travis, L. D.: Long term satellite record reveals likely recent aerosol trend, Science, 315, 1543, doi:10.1126/science.1136709, 2007.
North, P. R. J., Briggs, S. A., Plummer, S. E., and Settle, J. J., Retrieval of land surface bi-directional reflectance and aerosol opacity from ATSR-2multi-angle imagery, IEEE T. Geosci. Remote, 37, 526–537, 1999.
Omar, A. H., Won, J.-G., Winker, D. M., Yoon, S.-C., Dubovik, O., and McCormick, M. P.: Development of global aerosol models using cluster analysis of Aerosol Robotic Network (AERONET) measurements, J. Geophys. Res., 110, D10S14, doi:10.1029/2004JD004874, 2005.
Remer, L. A., Wald, A. E., and Kaufman, Y. J.: Angular and seasonal variation of spectral surface reflectance rations: implications for the remote sensing of aerosol over land, IEEE T. Geosci. Remote, 39, 275–283, 2001.
Remer, L. A., Tanre, D., Kaufman, Ichoku, Y. J., Mattoo, S., Levy, R., Chu, D. A., Holben, B., Dubovik, O., Smirnov, A., Martins, J. V., Li, R.-R., and Ahmad, Z.: Validation of MODIS aerosol retrieval over ocean. Geophys. Res. Lett., 29, 8008, doi:10.1029/2001GL013204, 2002.
Remer, L. A., Kaufman, Y. J., Tanre, D., Mattoo, S., Chu, D. A., Martins, J. V., Li, R. R., Ichoku, C., Levy, R. C., Kleidman, R. G., Eck, T. F., Vermote, E., and Holben, B. N.: The MODIS

ACPD
12, 4031–4071, 2012

aerosol algorithm, products, and validation, J. Atmos. Sci., 62, 947–973, 2005.
Rondeaux, G. and Herman, M.: Polarization of Light Reflected by Crop Canopies, Remote Sens. Environ., 38, 63–75, 1991.
Thieuleux, F., Moulin, C., Bréon, F. M., Maignan, F., Poitou, J., and Tanré, D.: Remote sensing of aerosols over the oceans using MSG/SEVIRI imagery, Ann. Geophys., 23, 3561–3568, doi:10.5194/angeo-23-3561-2005, 2005.
Thomas, G. E., Carboni, E., Sayer, A. M., Poulsen, C. A., Siddans, R., and Grainger R. G.: Oxford-RAL Aerosol and Cloud (ORAC): aerosol retrievals from satellite radiometers, in: Satellite Aerosol Remote Sensing over Land, edited by: Kokhanovsky, A. A. and de Leeuw, G., Chichester, UK: Praxis Publishing, 193–225, 2009.
Veefkind, J. P., de Leeuw, G., Durkee, P. A., Russell, P. B., Hobbs, P. V., and Livingston, J. M.: Aerosol optical depth retrieval using ATSR-2 and AVHRR data during TARFOX, J. Geophys. Res.- Atmos., 104, 2253–2260, 1999.
Wagner, S. C., Govaerts, Y. M., and Lattanzio, A.: Joint retrieval of surface reflectance and aerosol optical depth from MSG/SEVIRI observations with an optimal estimation approach: 2. Implementation and evaluation, J. Geophys. Res., 115, D02204, doi:10.1029/2009JD011780, 2010.
Xue, Y. and Cracknell, A. P.: Operational bi-angle approach to retrieve the Earth surface albedo from AVHRR data in the visible band, Int. J. Remote Sens., 16, 417–429, 1995.

ACPD
12, 4031–4071, 2012

Table 1. Properties of the spherical and non-spherical aerosol model in solar band of MSG/SEVIRI derived from AERONET observation (fine mode and coarse mode parameters come from Govaerts et al., 2011).

Aerosol	Label	Spherical			Non-spherical		
		ABSORB	MODABS	NONABS	SMARAD	MEDRAD	LARRAD
Fine mode	r_{vf}	0.155	0.221	0.179	0.145	0.172	0.202
	σ_f	0.404	0.497	0.426	0.500	0.636	0.627
	C_{vf}	0.083	0.094	0.101	0.037	0.033	0.043
	r_{ef}	0.143	0.195	0.164	0.129	0.141	0.165
Coarse mode	r_{vc}	3.012	2.886	3.004	2.423	1.961	1.978
	σ_c	0.649	0.598	0.623	0.617	0.549	0.527
	C_{vc}	0.051	0.050	0.039	0.262	0.364	0.521
	r_{ec}	2.414	2.427	2.474	1.984	1.672	1.697
S		98.6	93.6	98.5	3.1	1.3	1.2
g	0.6	0.58	0.68	0.62	0.68	0.72	0.74
	0.8	0.53	0.64	0.56	0.68	0.73	0.75
	1.6	0.56	0.58	0.51	0.70	0.74	0.78
ϖ	0.6	0.86	0.93	0.95	0.92	0.95	0.96
	0.8	0.834	0.92	0.94	0.93	0.96	0.97
	1.6	0.76	0.88	0.91	0.95	0.97	0.98

ACPD
12, 4031–4071, 2012

Table 2. Band solar irradiance at 1 AU (astronomical unit) (provided by EUMESAT).

Channel	Wavelength (μm)	Solar irradiance
1	0.8	65.2065
2	0.6	73.1869
3	1.6	61.9923

ACPD
12, 4031–4071, 2012

Table 3. Forty-two selected AERONET stations in Africa and Europe and their locations (latitude and longitude) for the aerosol retrieval validation.

Name	Longitude	Latitude	Elevation (m)
Arcachon	−1.163222	44.663528	11
ATHENS-NOA	23.775	37.988	130
Autilla	−4.603056	41.997222	873
Avignon	4.878067	43.93275	32
Banizoumbou	2.66475	13.541167	250
Blida	2.880556	36.508333	230
Cabauw	4.927	51.971	−1
Brussels	4.35	50.783332	120
Cabo_da_Roca	−9.5	38.783333	140
Carpentras	5.058333	44.083333	100
Chilbolton	−1.43698	51.14446	88
DMN_Maine_Soroa	12.023067	13.216717	350
Dunkerque	2.368117	51.03535	0
Eforie	28.632222	44.075	40
Ersa	9.359289	43.003669	80
FORTH_CRETE	25.282417	35.332694	20
Granada	−3.605	37.164	680
Hamburg	9.973333	53.568333	105
Helgoland	7.887361	54.177861	33
IER_Cinzana	−5.933867	13.278433	285
IFT-Leipzig	12.435278	51.3525	125
IMAA_Potenza	15.72	40.6	820
Ispra	8.6267	45.80305	235
Laegeren	8.351389	47.480278	735
Lampedusa	12.631667	35.516667	45
Lille	3.141667	50.611667	60
Mainz	8.3	49.999	150
Malaga	−4.4775	36.715	40
Minsk	27.601	53.92	200
Moldova	28.8156	47.0001	205
Palaiseau	2.208333	48.7	156
Paris	2.333333	48.866667	50
Rome_Tor_Vergata	12.647333	41.83955	130
Saada	−8.15583	31.62583	420
Salon_de_Provence	5.120278	43.605556	60
Seysses	1.259722	43.503333	179
Tamanrasset_INM	5.53	22.79	1377
Toulon	6.009444	43.135556	50
Venise	12.5083	45.3139	10
Villefranche	7.328889	43.683889	130
Wytham_Woods	−1.3325	51.770278	160
Zinder_Airport	8.990233	13.776683	456

ACPD
12, 4031–4071, 2012

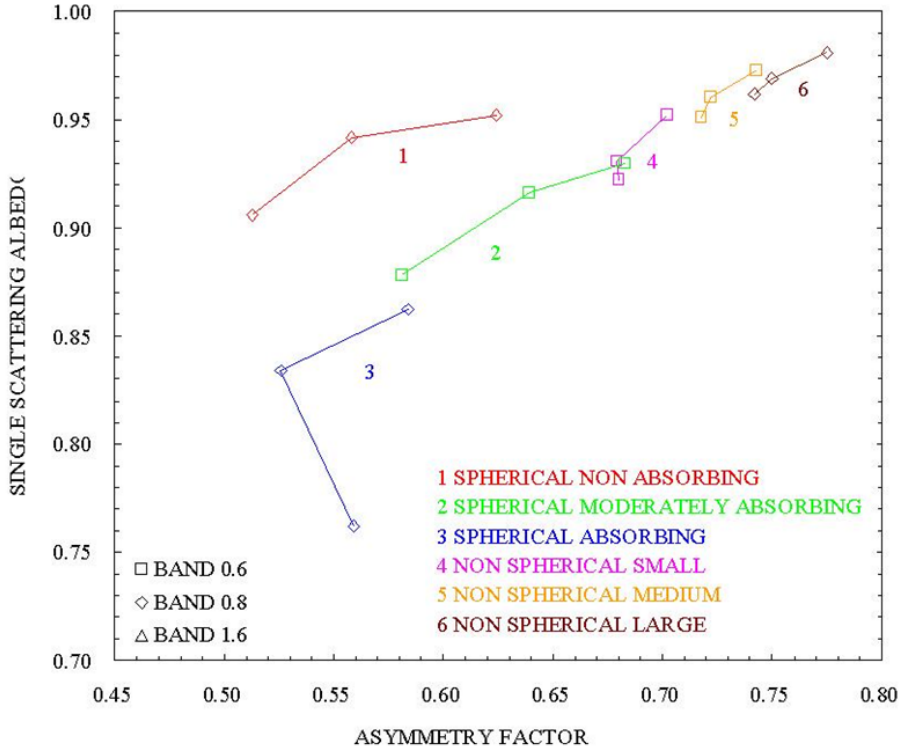

Fig. 1. Aerosol classes in the (g, ϖ) space derived from the analysis of AERONET observations at the SEVIRI solar channel wavelengths (Adapted from Govaerts et al., 2010).

ACPD
12, 4031–4071, 2012

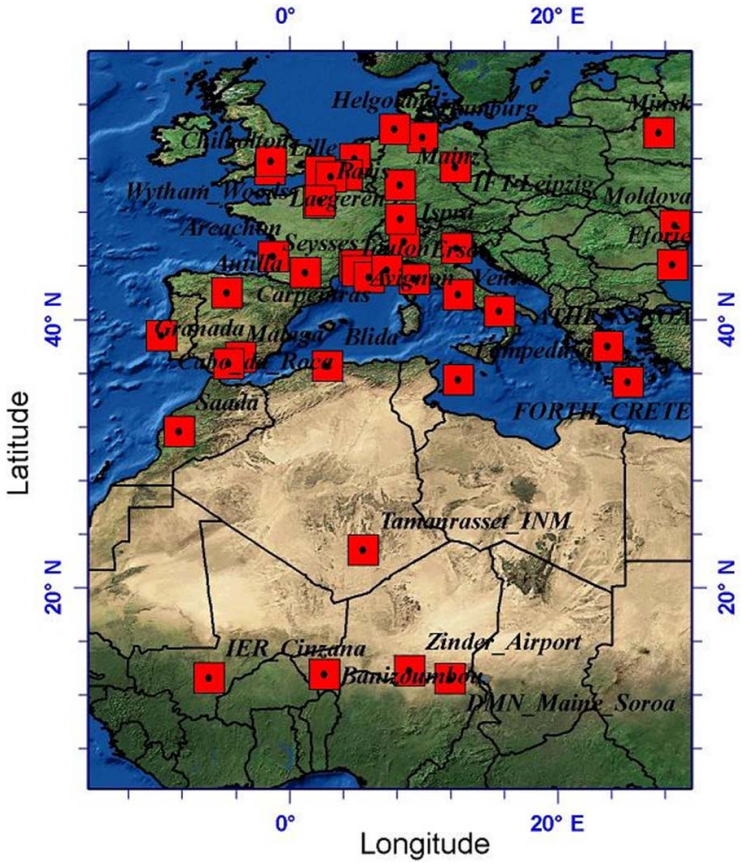

Fig. 2. AERONET chosen for validation in study area (red squares stand for AERONET) (−15°–30° E, 5°–60° N).

ACPD
12, 4031–4071, 2012

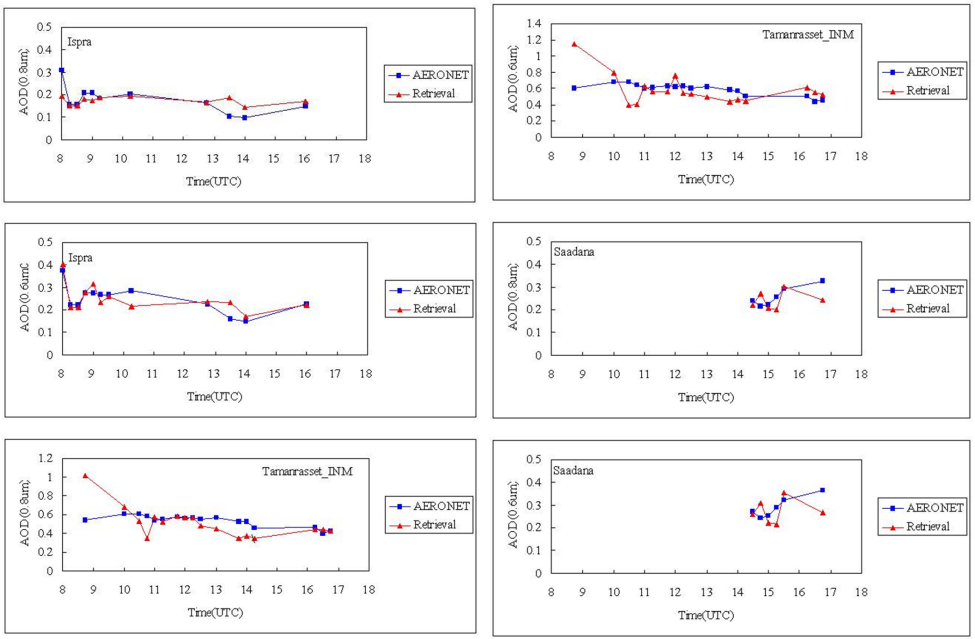

Fig. 3. Time-series of MSG/SEVIRI and AERONET AOD at 0.8 µm and 0.6 µm from 08:00 UTC to 18:00 UTC on 14 April 2010 at Tamanrasset_INM, Saada and IER_Cinzana sites.

ACPD
12, 4031–4071, 2012

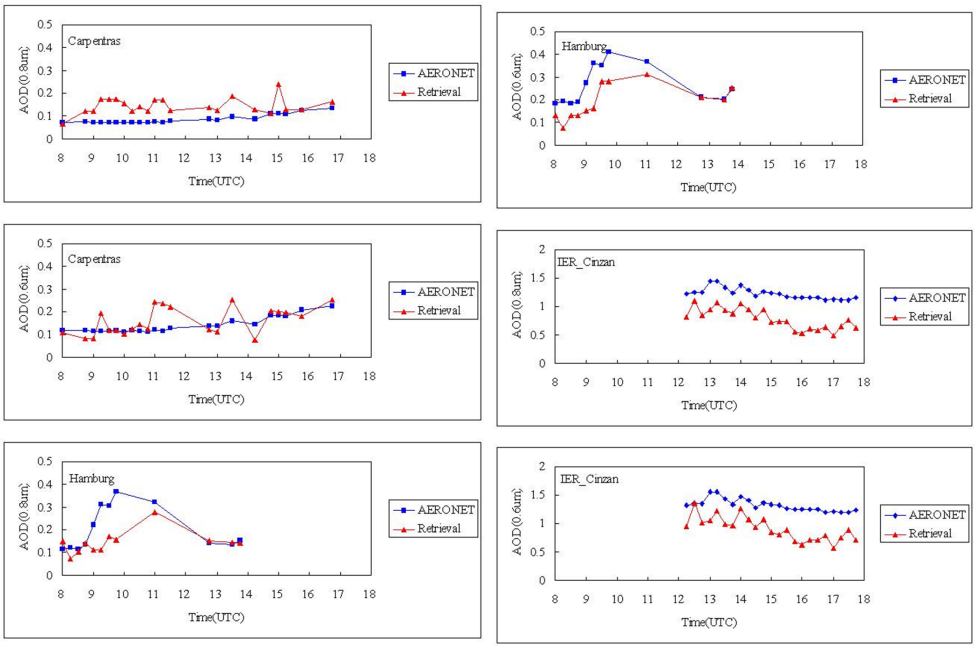

Fig. 3. Continued.

ACPD
12, 4031–4071, 2012

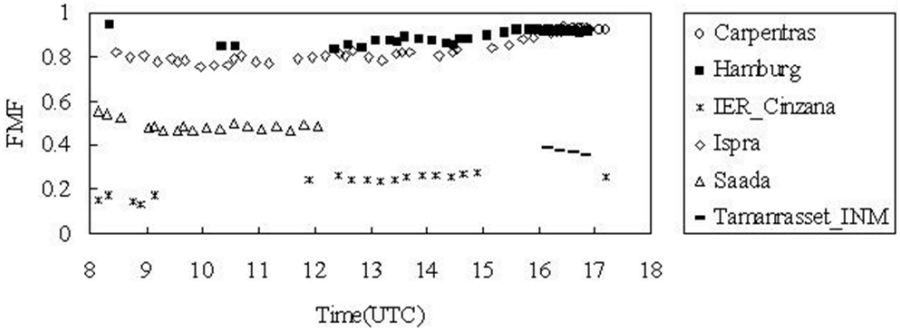

Fig. 4. Various FMF values measured between 08:00 and 18:00 UTC on 14 April 2010 at six selected AERONET sites.

ACPD
12, 4031–4071, 2012

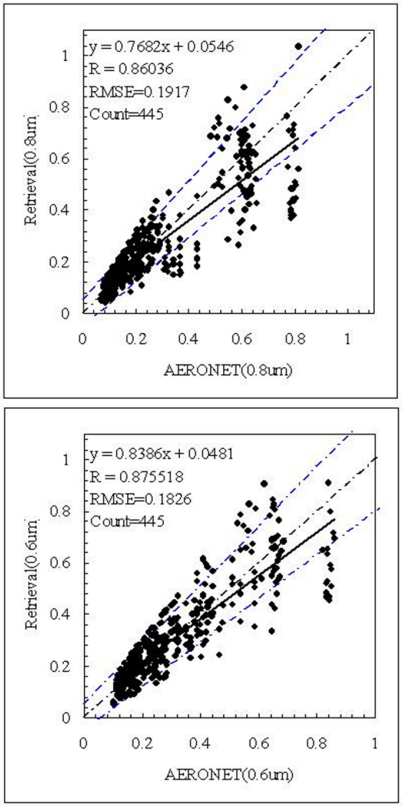

Fig. 5. Relationships between TS AOD and AERONET AOD at different wavelengths with a resolution of 10 km in the African area: **(a)** 0.8 µm, **(b)** 0.6 µm. The dashed (blue), dashed (black) and solid lines represent the error tolerance interval, the 1-1 line and the linear regression of the pre-sorted scatter plot, respectively. The text at the top describes the number of collocation (count), the regression curve, correlation (R), and the RMS error of the fit.

ACPD
12, 4031–4071, 2012

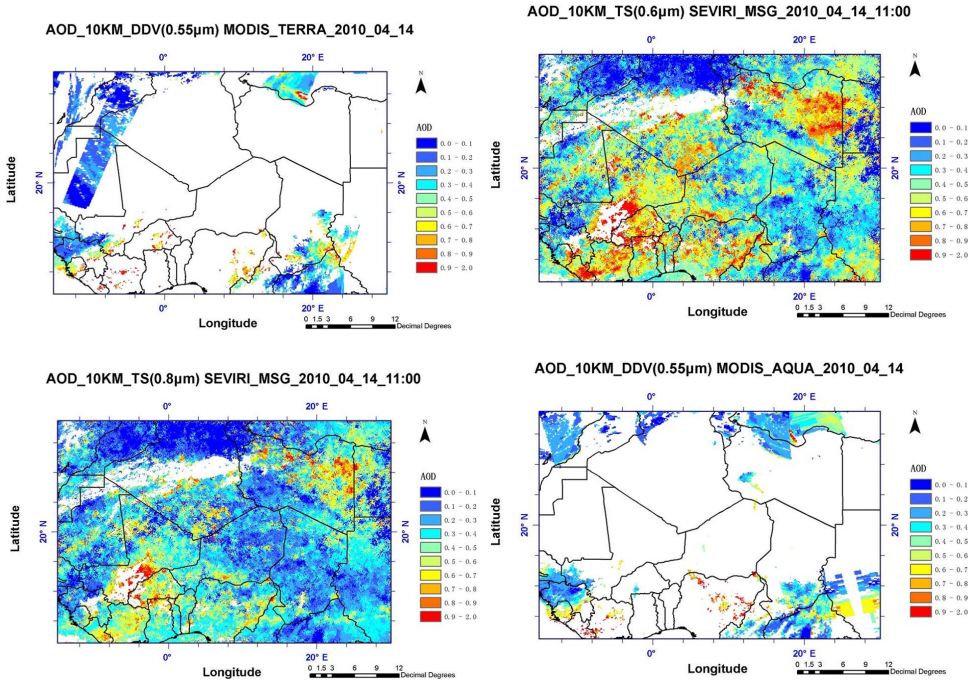

Fig. 6. **(a)** TERRA DDV AOD products; **(b)** TS AOD product of 0.6 μm at 11:00 UTC; **(c)** TS AOD product of 0.8 μm at 11:00 UTC; **(d)** AQUA DDV AOD product; **(e)** AQUA Deep Blue AOD product; **(f)** TS product of 0.8 μm at 15:30 UTC, and **(g)** TS product of 0.6 μm at 15:30 UTC with a 10 km resolution in the Africa area on 14 April 2010.

ACPD
12, 4031–4071, 2012

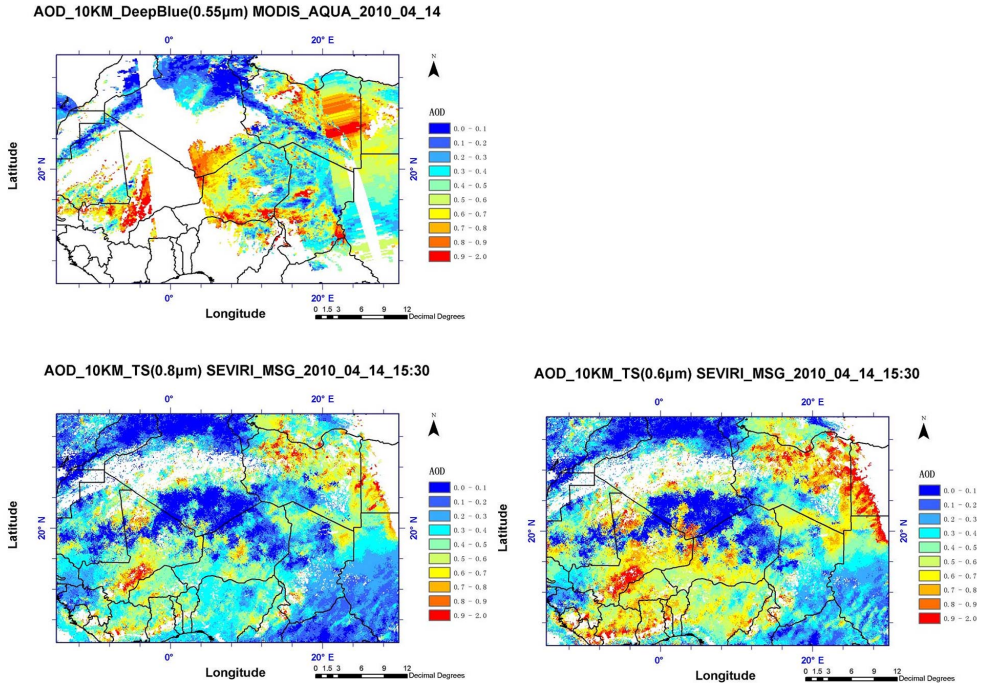

Fig. 6. Continued.

ACPD
12, 4031–4071, 2012

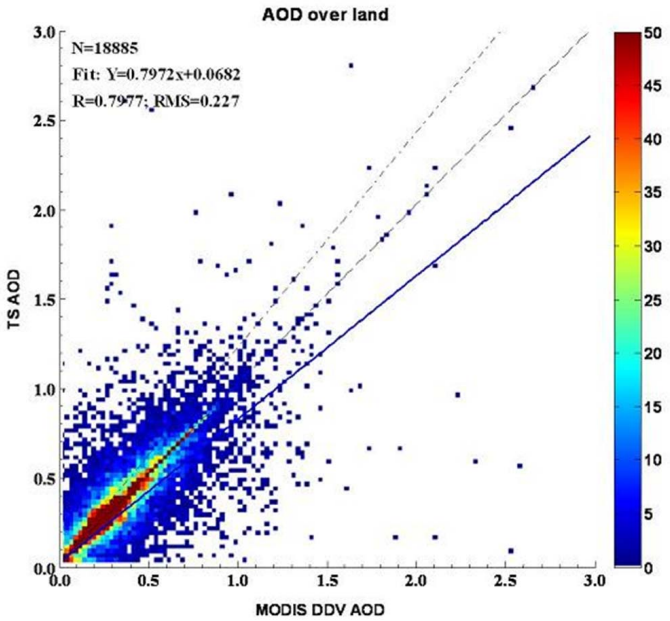

Fig. 7. Scatter plot of TS-derived data (0.6 µm) versus NASA DDV aerosol products for 0.55 µm of 10 × 10 km in the African area on 14 April 2010. Data are sorted according to ordered pairs (MODIS DDV AOD, TS AOD) of AOD in 0.02 intervals, and colour represents the number of cases (colour bar) with those particular ordered pair values. The dashed, dotted and solid lines are the 1-1 line, error tolerance interval and the linear regression of the pre-sorted scatter plot, respectively. The text at the top describes the number of collocation (*N*), the regression curve, correlation (*R*) and the RMS error of the fit.

ACPD
12, 4031–4071, 2012

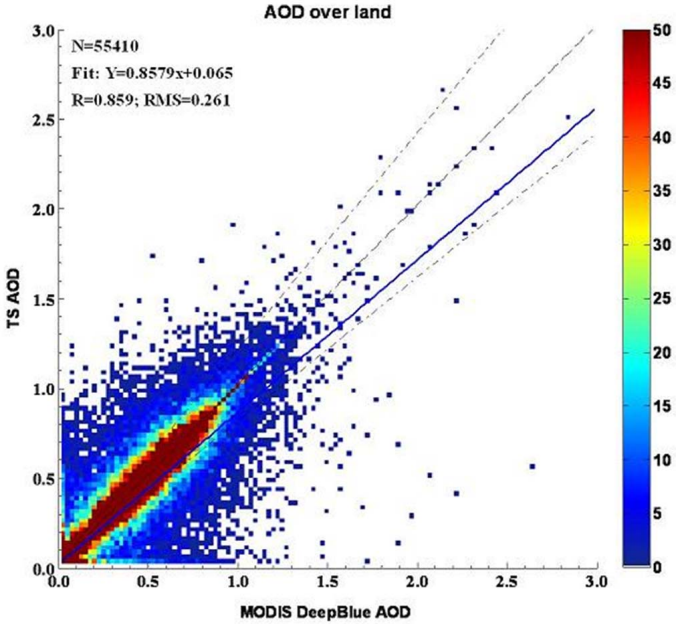

Fig. 8. Scatter plot of TS-derived data (0.6 µm) versus NASA Deep Blue aerosol products for 0.55 µm of 10 × 10 km in the African area on 14 April 2010. Data are sorted according to ordered pairs (MODIS Deep Blue AOD, TS AOD) of AOD in 0.02 intervals, and colour represents the number of cases (colour bar) with those particular ordered pair values. The dashed, dotted and solid lines are the 1-1 line, error tolerance interval and the linear regression of the presorted scatter plot, respectively. The text at the top describes the number of collocation (*N*), the regression curve, correlation (*R*) and the RMS error of the fit.

ACPD
12, 4031–4071, 2012

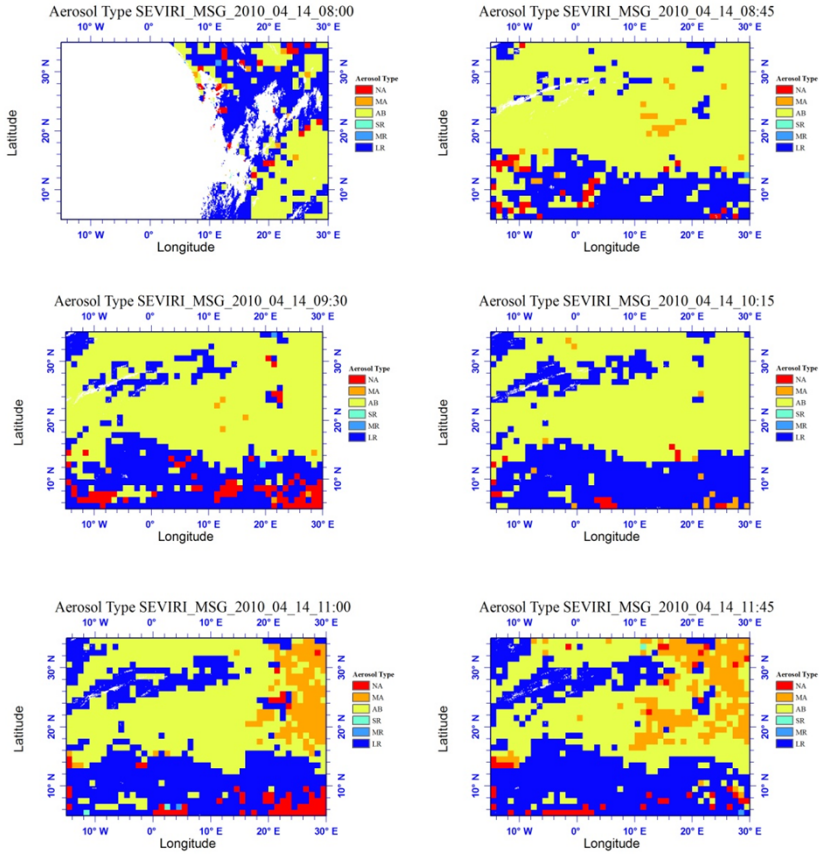

Fig. 9. Aerosol types in the African area on 14 April 2010 with time interval of 45 min. NA, MA, AB, SR, MR, LR stand for Spherical Non Absorbing, Spherical Moderately Absorbing, Spherical Absorbing, Non Spherical Small, Non Spherical Medium and Non Spherical Large respectively. The white area in the figure attributes to not data coverage.

ACPD
12, 4031–4071, 2012

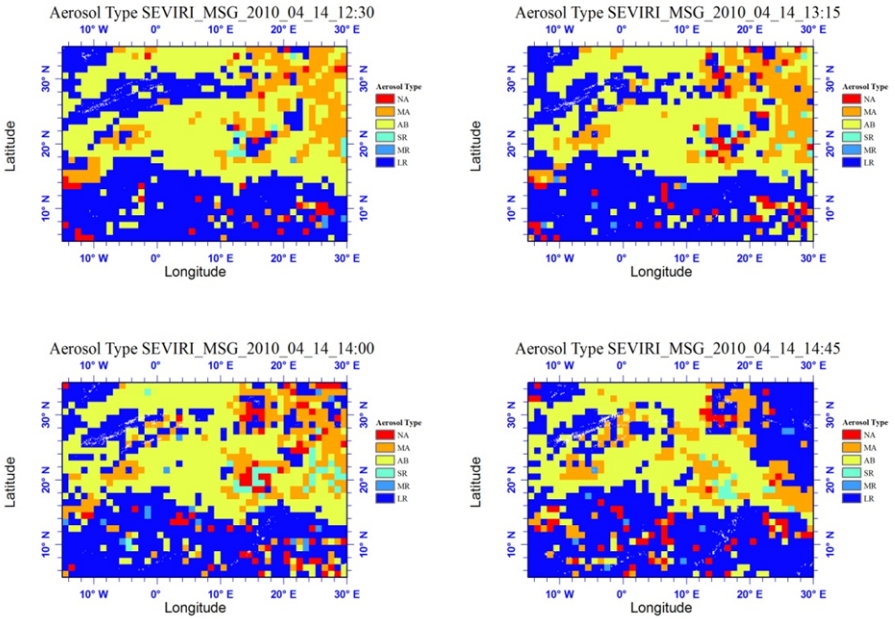

Fig. 9. Continued.

ACPD
12, 4031–4071, 2012

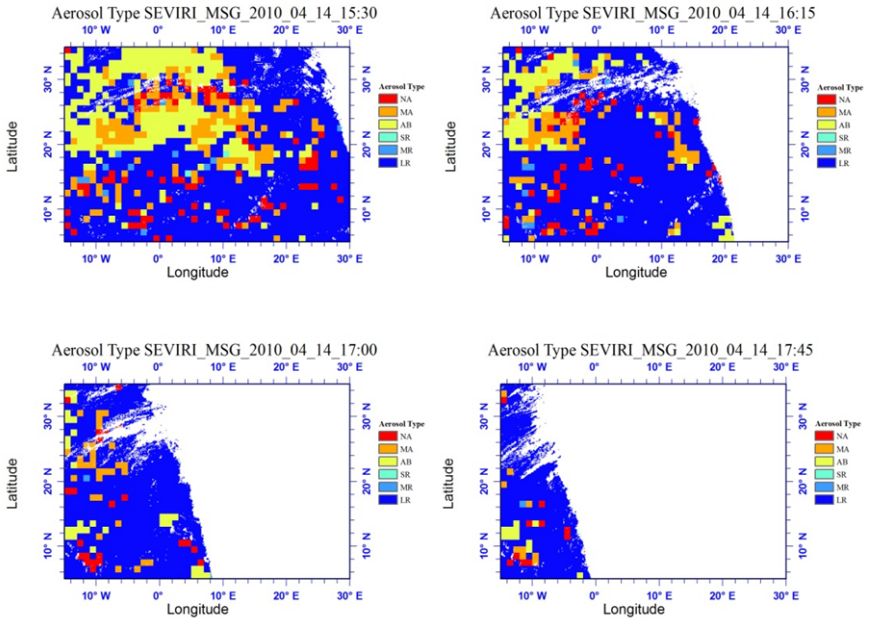

Fig. 9. Continued.

ACPD
12, 4031–4071, 2012